MDPI

*Article*

# RSM Modeling and Optimization of $CO_2$ Separation from High $CO_2$ Feed Concentration over Functionalized Membrane

Nadia Hartini Suhaimi [1,2], Yin Fong Yeong [1,2,*], Norwahyu Jusoh [1,2], Thiam Leng Chew [1,2], Mohammad Azmi Bustam [1,3] and Muhammad Mubashir [4]

[1] Department of Chemical Engineering, Universiti Teknologi PETRONAS, Bandar Seri Iskandar 32610, Malaysia; nadia_17005943@utp.edu.my (N.H.S.); norwahyu.jusoh@utp.edu.my (N.J.); thiamleng.chew@utp.edu.my (T.L.C.); azmibustam@utp.edu.my (M.A.B.)

[2] $CO_2$ Research Centre ($CO_2$RES), R&D Building, Universiti Teknologi PETRONAS, Bandar Seri Iskandar 32610, Malaysia

[3] Centre of Research in Ionic Liquids (CORIL), Universiti Teknologi PETRONAS, Bandar Seri Iskandar 32610, Malaysia

[4] Department of Petroleum Engineering, Faculty of Computing, Engineering & Technology, School of Engineering, Asia Pacific University of Technology, and Innovation, Kuala Lumpur 57000, Malaysia; mubashir@apu.edu.my

* Correspondence: yinfong.yeong@utp.edu.my

**Abstract:** The challenges in developing high $CO_2$ gas fields are governed by several factors such as reservoir condition, feed gas composition, operational pressure and temperature, and selection of appropriate technologies for bulk $CO_2$ separation. Thus, in this work, we report an optimization study on the separation of $CO_2$ from $CH_4$ at high $CO_2$ feed concentration over a functionalized mixed matrix membrane using a statistical tool, response surface methodology (RSM) statistical coupled with central composite design (CCD). The functionalized mixed matrix membrane containing $NH_2$-MIL-125 (Ti) and 6FDA-durene, fabricated in our previous study, was used to perform the separation performance under three operational parameters, namely, feed pressure, temperature, and $CO_2$ feed concentration, ranging from 3.5–12.5 bar, 30.0–50.0 °C and 15–70 mol%, respectively. The $CO_2$ permeability and $CO_2/CH_4$ separation factor obtained from the experimental work were varied from 293.2–794.4 Barrer and 5.3–13.0, respectively. In addition, the optimum operational parameters were found at a feed pressure of 12.5 bar, a temperature of 34.7 °C, and a $CO_2$ feed concentration of 70 mol%, which yielded the highest $CO_2$ permeability of 609.3 Barrer and a $CO_2/CH_4$ separation factor of 11.6. The average errors between the experimental data and data predicted by the model for $CO_2$ permeability and $CO_2/CH_4$ separation factor were 5.1% and 3.3%, respectively, confirming the validity of the proposed model. Overall, the findings of this work provide insights into the future utilization of $NH_2$-MIL-125 (Ti)/6FDA-based mixed matrix membranes in real natural gas purification applications.

**Keywords:** functionalized MOFs; high $CO_2$ concentration; optimization; RSM

## 1. Introduction

The East Natuna Block, located in the Greater Sarawak Basin near Natuna Island, Indonesia, is the largest natural gas field in Southeast Asia. It contains 46 trillion cubic feet (Tcf) of natural gas, and is identified as a high carbon dioxide ($CO_2$) content gas field, with $CO_2$ concentrations up to 70 mol%. In addition, about 13 trillion cubic feet (Tcf) of high $CO_2$ gas fields in Malaysia remain unexploited, with $CO_2$ concentrations of more than 40 mol%. According to the requirements of the gas processing plant, the $CO_2$ content should be reduced to 8 mol% in order to comply with the criteria of the downstream sales gas process [1]. High $CO_2$ contents can reduce the heating value of natural gas [2] and cause corrosion issues in pipelines in the presence of water [3]. Thus, it is crucial to investigate

technologies for separating $CO_2$ from methane at high $CO_2$ feed concentrations. Among conventional technologies such as absorption [4], adsorption [5], cryogenic distillation, and membrane separation [6], membrane separation has gained the most attention due to its small footprint, simple operation and energy efficiency [7].

The evolution of membrane materials in separation technology started with polymeric, followed by inorganic, mixed matrix and metal organic frameworks (MOFs), etc. Mixed matrix membranes comprised of polymeric material and inorganic filler were developed to address the trade-off in performance experienced by polymeric membranes [8] and reproducibility concerns regarding the fabrication of inorganic membranes [9]. Lately, incorporating MOF fillers in polymeric membranes for the formation of mixed matrix membranes has been the focus of many researchers due to the fact that the high porosity of MOF fillers can improve gas separation performance [10].

On top of that, numerous efforts have been made by researchers to further enhance the separation performance of mixed matrix membranes by functionalizing metal-organic frameworks (MOFs) fillers with $-NH_2$ functional groups. The presence of $-NH_2$ in the filler induces strong affinity toward $CO_2$ via hydrogen bonding, which enhances the interaction between $CO_2$ and the filler framework [11,12], and subsequently, improves the performance of the membrane in terms of $CO_2$ separation. Owing to its tunable pore size and affinity to $CO_2$ gas [13–15], $NH_2$-MIL-125 (Ti) has recently been studied as a filler for the formation of membranes for gas separation [3,16,17]. Previous studies reported that the separation performance of $NH_2$-MIL-125 (Ti)/polysulfone mixed matrix membranes was superior to that of neat polysulfone membranes [17]. This finding was attributed to the existence of porous fillers, which created an extra pathway for the penetration of $CO_2$ gas and promoted the diffusion of gas molecules through the membrane. Furthermore, in another work, a $NH_2$-MIL-125 (Ti)/Matrimid mixed matrix membrane was fabricated for $CO_2/CH_4$ separation and a $CO_2/CH_4$ gas pair selectivity of 50 was obtained when 15 wt% filler was loaded into the membrane [16]. This was mainly due to the small aperture size (6 Å) of $NH_2$-MIL-125 (Ti), which allowed $CO_2$ molecules to interact with the $-OH$ groups in Ti clusters, as well as interacting with $-NH_2$ groups on the linker. Also, our previous study discovered that the inclusion of $NH_2$-MIL-125 (Ti) filler in 6FDA-durene polymer matrices significantly improved the $CO_2$ permeability and $CO_2/CH_4$ gas pair selectivity, i.e., by 119% and 331%, respectively, compared to neat 6FDA-durene membranes [3]. The improvement in performance was mainly attributed to the high porosity of $NH_2$-MIL-125 (Ti) fillers and the attraction of amine functional groups to $CO_2$ molecules. Although several studies have been published on the utilization of functionalized MIL-125 (Ti) as a filler for the preparation of mixed matrix membranes in $CO_2/CH_4$ separation, these studies mostly focused on single gas permeation, binary gas separation (50:50) and the effect of feed pressure on the membrane performance [16,17]. Hence, further research evaluating the separation performance of the membrane at high $CO_2$ feed concentrations and various temperatures and $CO_2$ feed pressures in binary gas mixtures is still crucial.

According to the findings in the literature, operating temperature influences the $CO_2$ permeability of the membrane by affecting the mobility of the polymer chain and free volume [18] in the polymer, thus resulted in a change of $CO_2$ diffusivity [19]. In contrast, feed pressure may affect the gas solubility in the membrane, which affects the $CO_2$ permeability [11]. Furthermore, the $CO_2$ concentration in the feed can cause significant changes in $CO_2$ permeability through the membrane, which is mainly due to the higher sorption capability of $CO_2$ compared to $CH_4$. Hence, study of the correlation between the operational parameters and membrane separation performance is essential. In fact, several approaches, including response surface methodology (RSM), full factorial design and Taguchi methods, are available to investigate these questions.

For an experimental assessment and the optimization of the separation parameters, including significant responses and independent variables, comprehensive analytical tools and efficient optimization tools are practical. The multivariant method enabled the identification of the interaction between the variable parameters and responses. Furthermore, for our optimization study, the response surface methodology (RSM) was identified as the optimal tool. This technique combines the mathematical and statistical analyses by reducing the number of experiments. As a result, various researchers have reported the application of the RSM method in their studies.

Jusoh et al. [20] investigated the effect of pressure, temperature and $CO_2$ feed concentration on $CO_2/CH_4$ binary gas separation over a ZIF-8/6FDA-based mixed matrix membrane. They reported that the optimum parameter for $CO_2/CH_4$ separation performance was obtained at a feed pressure of 4.76 bar, a temperature of 30 °C, and a $CO_2$ feed concentration of 90 mol%. The latest study reported by Afarani et al. [18] utilized a polyurethane–zeolite 3A mixed matrix membrane to assess the impact of three independent variables, namely, zeolite content (0–24 wt%), operating temperature (25–45 °C), and operating pressure (0.2–0.1 MPa), on the single gas permeation performance. The optimum gas permeation performance of polyurethane–3A zeolite membrane was identified at a zeolite loading of 18 wt%, a temperature of 30 °C, and a pressure of 0.8 MPa. It can be observed that the RSM method has great potential for analyses of the relationship between the operational parameters and responses. Thus, the process of optimization of the separation performance over $NH_2$-MIL-125 (Ti)/6FDA-durene mixed matrix membranes by varying the operational parameters including feed pressure, temperature and $CO_2$ feed concentration using RSM method is presented in this study.

The 7.0 wt% $NH_2$-MIL-125 (Ti)/6FDA-durene mixed matrix membrane reported in our previous work [3] was used in this study, since the membrane demonstrated the best performance in $CO_2$ and $CH_4$ single gas permeation testing. First, the interaction of operational parameters, including feed pressure (A), temperature (B), and $CO_2$ feed concentration (C), toward the $CO_2$ and $CH_4$ permeability and $CO_2/CH_4$ separation factor were analyzed in detail using the RSM statistical method paired with the CCD optimization tool. Then, the significance of models was further evaluated by using analysis of variance (ANOVA). Next, 3D surface plots were used to visualize the linear, quadratic, and interaction between the operating parameters and significant responses. Subsequently, the optimum condition for the separation performance was generated and validated by experimental work.

## 2. Materials and Methods

### 2.1. Materials

Synthesis of $NH_2$-MIL-125 (Ti) fillers required trimethylacetic acid (99%), N,N-dimethylformamide (DMF), 2-aminoterephthalic acid (98%), terephthalic acid (98%), acetonitrile (99.8%) and tetraisopropyl ortthotitanate (97%). These chemicals were purchased from Sigma Aldrich (Missouri, MO, USA) and were used without further purification.

Synthesis of 6FDA-durene polyimide required two monomers, i.e., durene diamine (99%) and 6FDA dianhydride (99%). Durene diamine was purified through recrystallization using methanol, while 6FDA-dianhydride was purified via the vacuum sublimation technique. Vacuum distillation was used to purify N-methyl-2-pyrrolidone (NMP). Propionic anhydride ($\geq$98%), triethylamine ($\geq$99%), methanol ($\geq$99.9%) and dichloromethane ($\geq$99.8%) were purchased from Merck (Massachusetts, MA, USA) and were used as received.

The premixed gases used for the gas separation test were purchased from Air Products Sdn Bhd, (Kuala Lumpur, KL, Malaysia) with $CO_2$ compositions ranging from 15 mol% to 70 mol%.

### 2.2. Synthesis of 6FDA-Durene

In this study, 6FDA-durene polyimide was synthesized using a dual-step procedure reported in the literature [21]. First, equimolar amounts of durene diamine and 6FDA dianhydride monomers were dissolved in NMP for 24 h at room temperature under a nitrogen atmosphere. Next, polyimide was formed after adding propionic anhydride and triethylamine to the mixture solution. Then, the solution was precipitated in methanol and washed several times with methanol. The resulting polymer was dried under a vacuum for 24 h at 150 °C.

### 2.3. Synthesis of $NH_2$-MIL-125(Ti)

The $NH_2$-MIL-125 (Ti) filler was synthesized by following the method reported in our previous work [3]. Firstly, 17.5 g of pivalic acid was dissolved in a mixture solution containing 125 mL of acetonitrile and 5 mL of tetraisopropyl orthotitanate. Next, the mixture solution was placed in a Teflon-lined autoclave reactor and heated at 100 °C for 84 h to obtain white crystals. The white crystals were filtered and dried in an oven at 80 °C for 24 h. Then, 2.4 g of white crystals were dispersed in a mixture solution containing 50 mL methanol and 50 mL DMF. After that, the solution was added to a mixture solution containing 3.3 g of 2-aminoterephthalic acid and 75 mL of DMF. The final mixture was heated in an oven at 100 °C for 24 h. The resulting suspension was centrifuged at 7800 rpm for 5 min. Afterwards, the $NH_2$-MIL-125 (Ti) fillers were washed several times with methanol and DMF before being dried in an oven at 60 °C for 24 h.

### 2.4. Fabrication of Dense Membrane

In our previous work [3], the 7.0 wt% $NH_2$-MIL-125 (Ti) /6FDA-durene mixed matrix membrane showed the highest performance in terms of $CO_2$ and $CH_4$ single gas permeation; therefore, this membrane was utilized to obtain the optimum condition in $CO_2$/$CH_4$ binary gas separation. The mixed matrix membrane was prepared by dispersing fillers and dissolving the polymer in DCM separately. After stirring, the suspension was sonicated to disperse the fillers in DCM. Then, the priming step was introduced by adding 10 wt% of the polymer solution into the filler suspension under stirring to induce the polymer–filler interface [22] before the suspension was sonicated again. The remaining polymer solution was added to the suspension, which was then sonicated. Subsequently, the suspension was vigorously stirred for 1 h before being cast onto a petri dish. The petri dish was then covered with perforated aluminum foil for solvent evaporation at room temperature for 24 h. After complete evaporation, the membrane film was carefully removed from the petri dish and dried in an oven at 60 °C. Then, the membrane was further dried under vacuum at 60 °C for 24 h, followed by thermal annealing at 250 °C for 24 h.

### 2.5. Binary Gas Separation Measurement

Binary gas separation testing was carried out by using a custom-made permeation test rig as described in our previous work [3]. The compositions of gases in the retentate and permeate gas streams were determined using a gas analyzer (Fuji, NDIR Gas Analyzer ZPAJ). Then, the permeability of the gases was calculated using Equations (1) and (2), as follows [20]:

$$P_{CO2} = \frac{V_P y_{CO2} t}{A_m (p_h x_{CO2} - p_l y_{CO2})} \tag{1}$$

$$P_{CH4} = \frac{V_P y_{CH4} t}{A_m (p_h x_{CH4} - p_l y_{CH4})} \tag{2}$$

where $P_{CO2}$ and $P_{CH4}$ are the permeability of $CO_2$ and $CH_4$ (Barrer, 1 Barrer = $1 \times 10^{-10}$ cm$^3$ (STP).cm/s·cm$^2$·cmHg), $V_p$ is the volumetric flowrate (cm$^3$(STP)/s), $A_m$ and $t$ are the operational area (cm$^2$) and the thickness (cm) of the mixed matrix membrane, respectively, $p_h$ and $p_l$ are the pressure of feed and permeate side, respectively (cmHg), and $x$ and $y$

represent the volume fraction of the component in retentate and permeate streams by assuming ideal gas behaviors. The $CO_2/CH_4$ separation factor was calculated using Equation (3), as follows [20]:

$$\alpha_{CO_2/CH_4} = \frac{y_{CO_2}/y_{CH_4}}{x_{CO_2}/x_{CH_4}} \tag{3}$$

where $\alpha_{CO2/CH4}$ indicates the $CO_2/CH_4$ separation factor, and $x$ and $y$ represent the volume fraction of the component in the retentate and permeate streams, respectively.

### 2.6. Optimization of Membrane Separation Performance

The optimization of $CO_2$ separation from $CH_4$ was conducted based on the experimental runs generated by Design-Expert software V9.0 (Stat-Ease Inc., Minneapolis, MN, USA). The central composite design (CCD) available in the software was selected due to its various advantages, including its flexibility, efficiency, and continuous run. In the current study, three operational parameters were selected, namely, feed pressure (A), temperature (B), and $CO_2$ feed concentration (C). Meanwhile, three significant responses were determined, i.e., $CO_2$ permeability, $CH_4$ permeability and $CO_2/CH_4$ separation factor. All parameters were tested at three measurement levels from low to high range. Then, the alpha ($\alpha$) was fixed at 1, which is considered to be a face-centered design. The range and level of the operational parameters are shown in Table 1.

**Table 1.** Experimental range and levels of the operational parameters.

| Operational Parameters | Units | Coded Measurement Levels | | |
|---|---|---|---|---|
| | | −1 (Low) | 0 (Center) | 1 (High) |
| Feed Pressure (A) | Bar | 3.5 | 8.0 | 12.5 |
| Temperature (B) | °C | 30.0 | 40.0 | 50.0 |
| $CO_2$ Feed Concentration (C) | (mol%) | 15.0 | 42.5 | 70.0 |

The interaction between the operational parameters, i.e., feed pressure, temperature and $CO_2$ feed concentration, and responses, i.e., the permeability of the gases and the $CO_2/CH_4$ separation factor, were further analyzed via analysis of variance (ANOVA). The experimental results were fitted into empirical models (second-order polynomial function) expressed in Equation (4) in order to correlate the corresponding responses over the operational parameters [18].

$$Y = B_0 + \sum_{i=1}^{3} B_i x_i + \sum_{i=1}^{2} \sum_{j=i+1}^{3} B_{ij} x_i x_j + \sum_{i=1}^{3} B_{ii} x_i^2 \tag{4}$$

where $Y$ is the corresponding response, $B_0$ is a fixed term, and $B_i$, $B_{ij}$ and $B_{ii}$ are linear, interaction and quadratic terms, respectively. Meanwhile, $x_i$ and $x_j$ represent the coded terms for operational parameters.

The fitted model for each corresponding response was analyzed in terms of the statistical significance of the operational parameters and interactions using the F- and *p*-values. The F-value is defined as the ratio of the mean square model to the mean square error. The mean square model is the sum of squares divided by the number of degrees of freedom. The *p*-value indicates the significance of the model; therefore, $p < 0.05$ shows that the regression model is relevant, and the null hypothesis ($H_o$): $p \leq 0.5$ is rejected. In addition, the consistency of the models was quantified by the coefficient of determination ($R^2$). Residual is the unexplained variation by the fitted model. 'Lack of fit' denotes that the lack of fit is insignificant in comparison to the pure error.

## 3. Results and Discussion

### 3.1. Characteristics of Membrane

The physicochemical properties, morphology and filler distribution, thermal stability, fractional free volume (FFV) analysis as well as $CO_2$ and $CH_4$ single gas performance of the $NH_2$-MIL-125 (Ti)/6FDA-durene membranes at various filler loadings were discussed in detail in our previous work [3]. As noted in our previous work, the 7.0 wt% $NH_2$-MIL-125 (Ti)/6FDA-durene mixed matrix membrane exhibited the highest $CO_2$ permeability and $CO_2/CH_4$ gas pair selectivity, i.e., 1115.7 Barrer and 37.1, respectively, at a feed pressure of 3.5 bar and at room temperature. In this work, the performance of this membrane in mixed gas separation with various operating parameters, particularly at high $CO_2$ feed concentration, was investigated using a statistical approach consisting of a central composite design (CCD) paired with a response surface methodology (RSM). Figure S1 and Table S1 display the characterization results comprising the XRD, FESEM, EDX and FFV for the 7.0 wt% $NH_2$-MIL-125 (Ti)/6FDA-durene mixed matrix membrane. In reference to Figure S1a, the significant peaks observed at 6.9° and 9.8° corresponded to the X-ray reflection planes (011) and (002) of the $NH_2$-MIL-125 (Ti) fillers. Meanwhile, the fillers were encapsulated and uniformly dispersed in the 6FDA-durene polymer matrix, as shown in Figure S1b. On the other hand, Table S1 compares the $CO_2$ and $CH_4$ single gas permeation performance and FFV values of pure and 7.0 wt% $NH_2$-MIL-125 (Ti)/6FDA-durene mixed matrix membrane.

### 3.2. Central Composite Design (CCD)

From CCD, 20 trial experiments, including eight factorial points, six axial points, and six central point replicates in a randomized sequence, were generated by the DoE software. The replicated center points were used to estimate the pure error for the lack of fit test. The randomized sequence for the experimental run was intended to limit the impact of uncontrollable factors. Therefore, experimental 20 runs were conducted and three significant responses, namely, $CO_2$ permeability, $CH_4$ permeability, and $CO_2/CH_4$ separation factor, were measured. Table 2 shows the condition of the operational parameters and significant responses of the membrane separation performance observed in the experiments. From Table 2, it can be observed that the permeability of $CO_2$ and $CH_4$ were in the range of 293.2 to 794.4 Barrer and 28.7 to 147.5 Barrer, respectively. The percentage errors between the actual and predicted values of membrane separation performances are listed in Table S2.

**Table 2.** CCD design matrix of $2^3$ factorial generated by DOE and the obtained significant responses.

| | Operational Parameters | | | Significant Responses | | |
|---|---|---|---|---|---|---|
| Run | A: Pressure (Bar) | B: Temperature (°C) | C: $CO_2$ Concentration (mol%) | $CO_2$ Permeability (Barrer) | $CH_4$ Permeability (Barrer) | $CO_2/CH_4$ Separation Factor |
| 1 | 3.5 | 40.0 | 42.5 | 569.6 | 58.3 | 9.9 |
| 2 | 8.0 | 40.0 | 42.5 | 569.6 | 58.3 | 9.9 |
| 3 | 3.5 | 50.0 | 70.0 | 326.2 | 52.3 | 5.5 |
| 4 | 12.5 | 30.0 | 70.0 | 609.1 | 81.9 | 7.3 |
| 5 | 8.0 | 40.0 | 70.0 | 450.2 | 92.7 | 6.0 |
| 6 | 8.0 | 50.0 | 42.5 | 504.0 | 39.9 | 12.8 |
| 7 | 3.5 | 30.0 | 70.0 | 448.2 | 33.9 | 13.0 |
| 8 | 12.5 | 50.0 | 70.0 | 293.2 | 36.2 | 7.3 |
| 9 | 12.5 | 30.0 | 15.0 | 506.6 | 83.2 | 6.1 |
| 10 | 8.0 | 40.0 | 15.0 | 419.7 | 39.7 | 8.6 |
| 11 | 12.5 | 40.0 | 42.5 | 794.4 | 147.5 | 5.3 |
| 12 | 8.0 | 40.0 | 42.5 | 442.9 | 39.5 | 8.6 |
| 13 | 3.5 | 50.0 | 15.0 | 502.3 | 47.4 | 10.8 |

**Table 2.** *Cont.*

| Run | Operational Parameters | | | Significant Responses | | |
|---|---|---|---|---|---|---|
| | **A: Pressure (Bar)** | **B: Temperature (°C)** | **C: CO$_2$ Concentration (mol%)** | **CO$_2$ Permeability (Barrer)** | **CH$_4$ Permeability (Barrer)** | **CO$_2$/CH$_4$ Separation Factor** |
| 14 | 8.0 | 40.0 | 42.5 | 321.5 | 28.7 | 11.4 |
| 15 | 3.5 | 30.0 | 15.0 | 464.4 | 58.4 | 8.1 |
| 16 | 8.0 | 30.0 | 42.5 | 650.2 | 97.0 | 8.4 |
| 17 | 8.0 | 40.0 | 42.5 | 520.3 | 55.5 | 9.3 |
| 18 | 12.5 | 50.0 | 15.0 | 567.5 | 74.3 | 7.5 |
| 19 | 8.0 | 40.0 | 42.5 | 520.3 | 55.5 | 9.3 |
| 20 | 8.0 | 40.0 | 42.5 | 510.1 | 91.0 | 6.1 |

Meanwhile, the CO$_2$/CH$_4$ separation factor obtained ranged from 5.6 to 13.0. The margin of error of the experimental results was ±5%. Furthermore, compared to single gas permeation testing [3], the performance of the membrane in binary gas separation demonstrated lower values. These difference could be explained by the competitive sorption between CO$_2$ and CH$_4$ gas molecules [23]. The presence of a competitive gas may substantially affect the gas penetration over the membrane [24].

*3.3. CO$_2$ Permeability*

The quadratic polynomial model suggested by the DoE software for CO$_2$ permeability is shown in Equation (5) in the form of a coded value.

$$CO_2 Permeability_{coded} = 518.31 - 67.77A + 36.63B + 98.10C - 72.10AB - 33.77AC + 16.25BC + 28.97A^2 - 117.49B^2 + 50.49C^2 \tag{5}$$

where *A*, *B* and *C* denote the feed pressure (bar), temperature (°C) and CO$_2$ feed concentration (mol%), respectively.

Table 3 presents the findings of the ANOVA and regression analysis for CO$_2$ permeability over the membrane. As shown in Table 3, model F and *p* values of 27.11 and <0.05 were achieved, respectively, suggesting that the model is statistically significant. In this case, *A*, *B*, *C*, *AB*, *AC*, *B$^2$*, *C$^2$* are statistically significant model terms. It can be observed from Table 3 that an R$^2$ value of 0.96 was achieved, which validated the accuracy of the model for CO$_2$ permeability.

**Table 3.** Analysis of variance (ANOVA) for CO$_2$ permeability.

| Source | Sum of Squares | Degree of Freedom | Mean Square | F-Value | Prob > F |
|---|---|---|---|---|---|
| Model | 2.471 × 10$^5$ | 9 | 27,456.76 | 27.11 | <0.0001 [a] |
| A-Pressure | 45,922.31 | 1 | 45,922.31 | 45.34 | <0.0001 [a] |
| B-Temperature | 13,418.30 | 1 | 13,418.30 | 13.25 | 0.0045 [a] |
| C-Concentration | 96,228.25 | 1 | 96,228.25 | 95.00 | <0.0001 [a] |
| AB | 41,584.40 | 1 | 41,584.40 | 41.05 | <0.0001 [a] |
| AC | 9123.30 | 1 | 9123.30 | 9.01 | 0.0133 [a] |
| BC | 2111.85 | 1 | 2111.85 | 2.08 | 0.1794 [b] |
| A$^2$ | 2307.53 | 1 | 2307.53 | 2.28 | 0.1621 [b] |
| B$^2$ | 37,959.26 | 1 | 37,959.26 | 37.47 | 0.0001 [a] |
| C$^2$ | 7009.65 | 1 | 7009.65 | 6.92 | 0.0251 [a] |
| Residual | 10,129.32 | 10 | 1012.93 | | |
| Lack of Fit | 5282.07 | 5 | 1056.41 | 1.09 | 0.4636 [b] |
| R$^2$ | 0.96 | | | | |

[a] statistically significant, [b] statistically not significant.

Figure 1a–c display a 3D plot of the effect of different operational parameters on $CO_2$ permeability. The increment of temperature at a feed pressure of 3.5 bar and a fixed $CO_2$ feed concentration of 42.5 mol% resulted in higher $CO_2$ permeability, as observed in Figure 1a. This could be due to the higher $CO_2$ diffusivity [19] caused by the increment of polymer chain mobility and free volume [18]. Meanwhile, the increment of feed pressure at temperatures between 30 to 40 °C resulted in a slight improvement in $CO_2$ permeability due to the increase in gas solubility as a consequence of thermodynamic promotion [11]. On the other hand, a decreasing trend of $CO_2$ permeability can be seen for temperatures ranging from 40 to 50 °C, mainly because of the $CO_2$ sorption isotherm, which follows the dual-mode sorption mechanism [25]. Generally, higher temperatures lead to higher $CO_2$ permeability; however, in this study, we observed a different trend. This might have been related to the lower solubility of gas molecules with increasing temperature. The adverse impact of temperature on sorption enthalpy would have affected the transport and sorption behavior of gases over the membrane [26]. From the obtained results, a maximum $CO_2$ permeability of 609.1 Barrer was achieved at a feed pressure of 3.5 bar and a temperature of 40 °C. Meanwhile, the lowest $CO_2$ permeability, i.e., 321.5 Barrer, was achieved at a feed pressure of 8 bar and a temperature of 30 °C.

Figure 1b shows the effect of $CO_2$ feed concentration and feed pressure on $CO_2$ permeability at a constant temperature of 40 °C. It can be seen in Figure 1b that the lowest $CO_2$ permeability, i.e., 470.7 Barrer, was achieved at a $CO_2$ feed concentration of 15 mol% and a feed pressure of 8 bar. In contrast, the highest $CO_2$ permeability, 792.2 Barrer, was obtained at a feed pressure of 3.5 bar and a $CO_2$ feed concentration of 70 mol%. Additionally, at constant temperature, increasing the $CO_2$ feed concentration in the feed caused significant improvement in $CO_2$ permeability; this was mainly due to the higher sorption of $CO_2$ than $CH_4$ over the membrane. Furthermore, the interaction between $CO_2$ molecules and $-NH_2$ elements also contributed to the improvement of $CO_2$ diffusion through the membrane [27]. On the other hand, the $CO_2$ permeability decreased slightly with increasing feed pressure. This result was attributed to the saturation of available sorption sites, which resulted in a lower solubility coefficient [28]. Furthermore, this trend was also related to the dual-mode sorption and diffusion mechanism on gas transport behavior over the membrane.

Figure 1c illustrates the effect of $CO_2$ feed concentration and temperature on $CO_2$ permeability at a fixed feed pressure of 8 bar. As shown in Figure 1c, increasing the $CO_2$ feed concentration led to an increase in $CO_2$ permeability due to the higher $CO_2$ sorption effect relative to $CH_4$, which, subsequently, enhanced the sorption of $CO_2$ over $CH_4$ gas molecules in the membrane. A similar incremental trend of $CO_2$ permeability was observed under fixed feed pressure conditions, as shown in Figure 1b. When the temperature increased from 30 °C to 40 °C at a constant feed pressure of 8 bar, the $CO_2$ permeability improved due to the increase in movement and flexibility of polymer chains, as well as the kinetic energy of gas molecules [26]. Furthermore, it could be that the impact of temperature on the gas transport and the sorption behavior compensated for the adverse effect of temperature on gas solubility. However, a slight decrease in $CO_2$ permeability was discovered after increasing the temperature from 40 °C to 50 °C. This was mainly due to the sorption competition between the $CO_2$ and $CH_4$ gases [25]. The reduction in gas solubility caused by the reduced interaction of $CO_2$ gas with the polymer matrix was attributed to the increment of adsorption energy with temperature; consequently, the thermodynamic effect overcame the kinetic effect during gas penetration [29]. From Figure 1c, it may be seen that the maximum $CO_2$ permeability, i.e., 650.2 Barrer, was achieved at a feed pressure of 8 bar, a $CO_2$ feed concentration of 70 mol% and a temperature of 40 °C. A parity plot for $CO_2$ permeability is shown in Figure S2a. It can be seen that the actual and predicted values of the responses were scattered near to the 95% prediction limits.
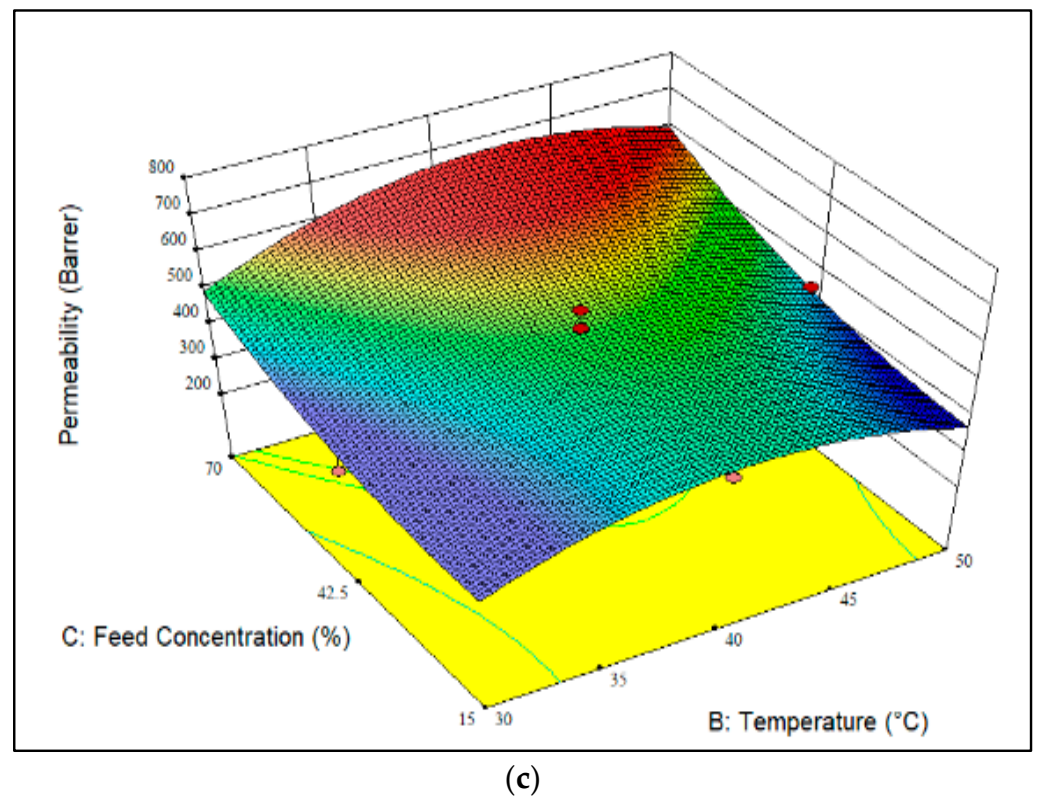
(**a**)



(**b**)

**Figure 1.** *Cont.*

**(c)**
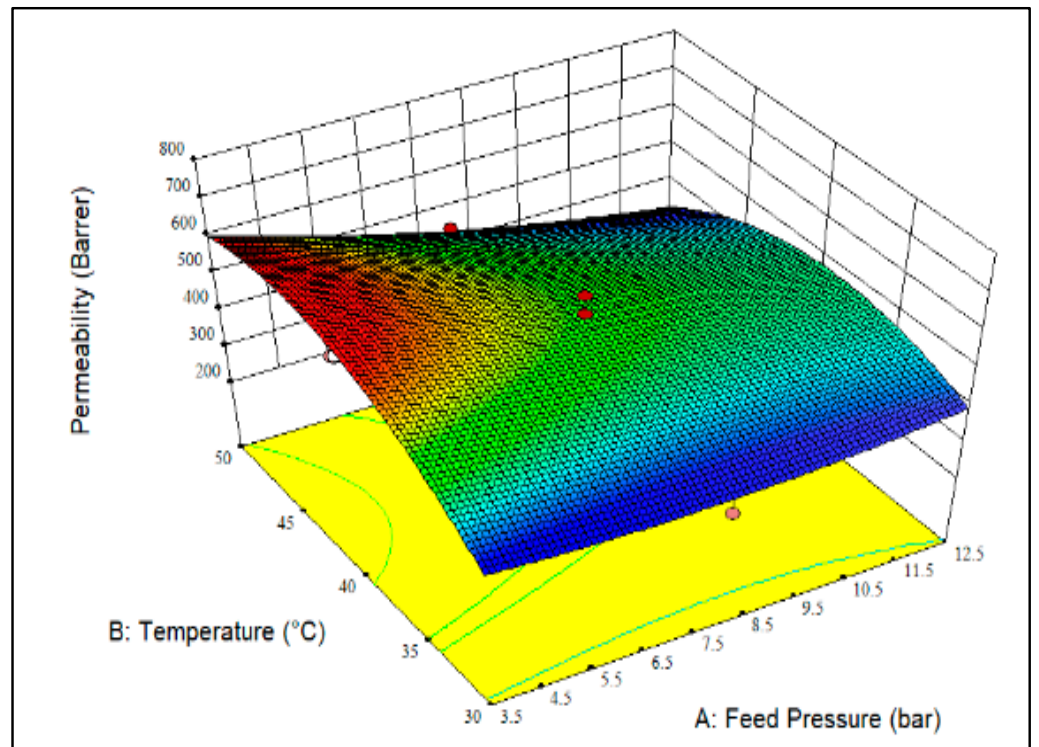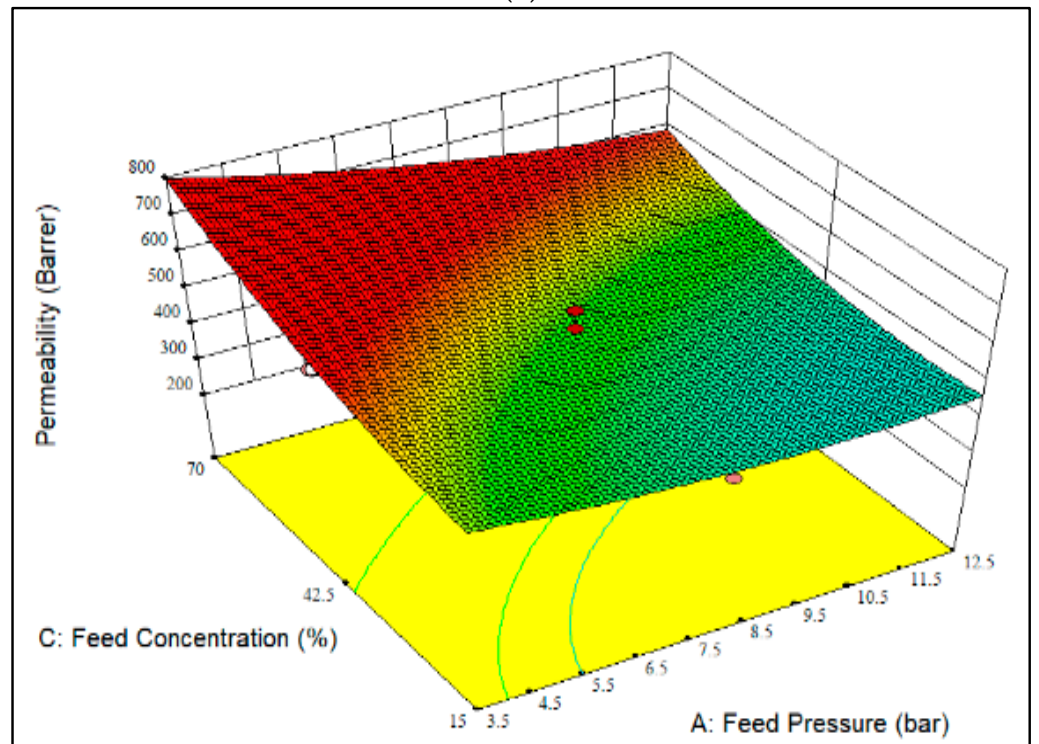
**Figure 1.** 3D surface of the $CO_2$ permeability as a function of feed pressure, $CO_2$ feed concentration and temperature at (**a**) $CO_2$ feed concentration of 42.5 mol%, (**b**) temperature of 40 °C and (**c**) feed pressure of 8 bar. (The darker colour (red) representing higher membrane performance whereas a lighter colour (blue) indicating lower membrane performance).

*3.4. CH$_4$ Permeability*

Equation (6) depicts the quadratic polynomial model for $CH_4$ permeability in terms of coded value.

$$CH_4 Permeability_{coded} = 55.48 - 23.89A + 13.76B + 10.52C - 12.10AB - 7.01AC + 7.08BC - 0.15A^2 - 24.03B^2 + 36.76C^2 \tag{6}$$

where *A*, *B* and *C* denote the feed pressure (bar), temperature (°C) and $CO_2$ feed concentration (mol%), respectively.

Table 4 demonstrates the ANOVA and regression analysis of $CH_4$ permeability. As shown, F and *p* values of 29.95 and < 0.05, respectively, were achieved, indicating that the model terms were statistically significant. Additionally, *A*, *B*, *C*, *AB*, *AC*, *BC*, *B$^2$* and *C$^2$* were statistically significant model terms in this context. In addition, an $R^2$ value of 0.96 was obtained, confirming the accuracy of the model for $CH_4$ permeability.

**Table 4.** Analysis of variance (ANOVA) for $CH_4$ permeability.

| Source | Sum of Squares | Degree of Freedom | Mean Square | F-Value | Prob > F |
|---|---|---|---|---|---|
| Model | 15,005.47 | 9 | 1667.27 | 29.95 | <0.0001 [a] |
| A-Pressure | 5708.28 | 1 | 5708.28 | 102.54 | <0.0001 [a] |
| B-Temperature | 1892.55 | 1 | 1892.55 | 34.00 | 0.0002 [a] |
| C-Concentration | 1106.91 | 1 | 1106.91 | 19.88 | 0.0012 [a] |
| AB | 1171.28 | 1 | 1171.28 | 21.04 | 0.0010 [a] |
| AC | 393.68 | 1 | 393.68 | 7.07 | 0.0239 [a] |
| BC | 400.73 | 1 | 400.73 | 7.20 | 0.0230 [a] |

**Table 4.** *Cont.*

| Source | Sum of Squares | Degree of Freedom | Mean Square | F-Value | Prob > F |
|--------|----------------|-------------------|-------------|---------|----------|
| $A^2$ | 0.066 | 1 | 0.066 | $1.180 \times 10^{-3}$ | 0.9733 [b] |
| $B^2$ | 1587.90 | 1 | 1587.90 | 28.52 | 0.0003 [a] |
| $C^2$ | 3716.16 | 1 | 3716.16 | 66.75 | <0.0001 [a] |
| Residual | 556.69 | 10 | 55.67 | | |
| Lack of Fit | 429.72 | 5 | 85.94 | 3.38 | 0.1035 [b] |
| $R^2$ | 0.96 | | | | |

[a] statistically significant, [b] statistically not significant.

Figure 2a–c display a 3D plot of the $CH_4$ permeability over the membrane. The increment of temperature from 30 °C to 40 °C resulted in higher $CH_4$ permeability, as observed in Figure 2a. The increase in chain mobility and free volume resulted in higher diffusivity, and thus, increased the penetration of $CH_4$ molecules through the membrane [30]. The relationship between temperature and permeability can be defined using Arrhenius equation, where $CH_4$ molecules exhibit higher activation energy than $CO_2$ molecules, and therefore, promote the diffusion of nonpolar gases over the glassy polymer. Meanwhile, a reduction of $CH_4$ permeability was found with the increment of temperature from 40 °C to 50 °C. This was ascribed to the reduction in solubility, which subsequently enhanced the restriction of $CH_4$ gas permeation through the membrane [31]. Meanwhile, increasing the feed pressure caused a slight reduction in $CH_4$ permeability, mainly due to the decrease in the dual-sorption properties for $CH_4$ gas [19], as well as the high compressibility of $CH_4$ gas molecules [32] in the membrane.

Figure 2b shows the effect of $CO_2$ feed concentration and feed pressure on $CH_4$ permeability at a constant temperature of 40 °C. Referring to Figure 2b, the $CH_4$ permeability obtained at feed pressures ranging from 3.5 bar to 12.5 bar demonstrated a similar trend to the results presented in Figure 2a. On the other hand, an increase in $CO_2$ feed concentration from 15 mol% to 42.5 mol% led to a reduction of $CH_4$ permeability, due to the lower sorption of $CH_4$ compared to $CO_2$, as well as the slower diffusion of $CH_4$ gas over the membrane [20]. However, increasing the $CO_2$ feed concentration from 42.5 mol% to 70 mol% enhanced the permeability of $CH_4$. The increasing trend in $CH_4$ permeability was because of the swelling of polymer chain packing at higher $CO_2$ feed concentrations, and therefore, increased the segmental mobility [19]. On the other hand, the lowest $CH_4$ permeability, i.e., 33.9 Barrer, was seen with a $CO_2$ feed concentration of 42.5 mol% and a feed pressure of 12.5 bar. In contrast, the maximum $CH_4$ permeability, 133.3 Barrer, was achieved at a $CO_2$ feed concentration of 70 mol%, a temperature of 40 °C and a feed pressure of 3.5 bar (Figure 2b).

Figure 2c demonstrates the effect of $CO_2$ feed concentration and temperature on $CH_4$ permeability at a constant feed pressure of 8 bar. As shown, the $CH_4$ permeability gradually improved with increasing the temperature, owing to the enhanced mobility and flexibility of the polymer chains [26], as well as to the higher activation energy of $CH_4$ [33]. Meanwhile, a reduction in $CH_4$ permeability was observed at $CO_2$ feed concentrations ranging from 15 mol% to 42.5 mol%, and an improvement in $CH_4$ permeability was found when the $CO_2$ feed concentration increased from 42.5 mol% to 70 mol%. This trend was identical to that shown in Figure 2b. Apart from that, the highest $CH_4$ permeability, i.e., 106.1 Barrer, was obtained with a $CO_2$ feed concentration of 70 mol%, a feed pressure of 8 bar and a temperature of 40 °C (Figure 2c); this was associated with concentration polarization effects [34]. Meanwhile, the lowest $CH_4$ permeability, 28.7 Barrer, was observed at a $CO_2$ feed concentration of 42.5 mol% and a temperature of 30 °C. The increase in $CH_4$ permeability with the increase in temperature and $CO_2$ feed concentration was mainly due to the increase in polymer free volume caused by the alteration of polymer chain packing and intersegmental motion [33], as well as the swelling effect induced by $CO_2$ gas. The presence of high $CO_2$ feed concentrations caused the rapid diffusion of $CH_4$ gas through

the membrane [35], because $CH_4$ gas molecules are more accessible to a swollen polymer matrix. A parity plot for $CH_4$ permeability is shown in Figure S2b. As shown, very few data points fall outside the 95% prediction limits.
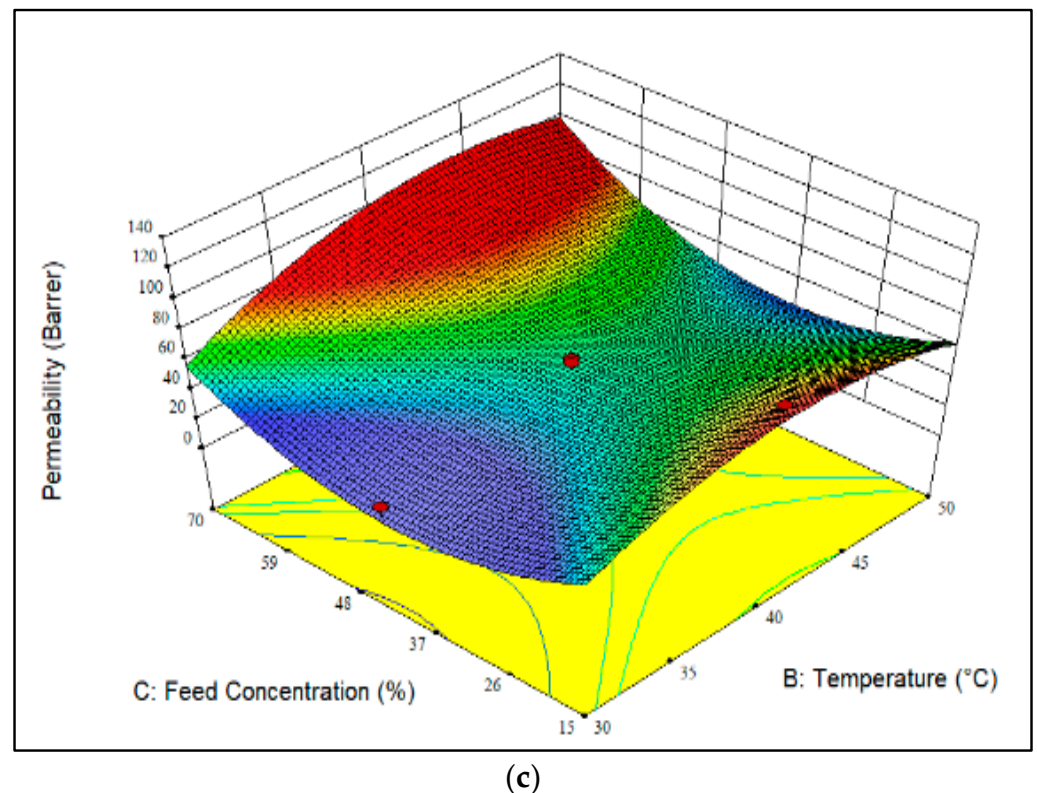


(**a**)



(**b**)

**Figure 2.** *Cont*.

**(c)**
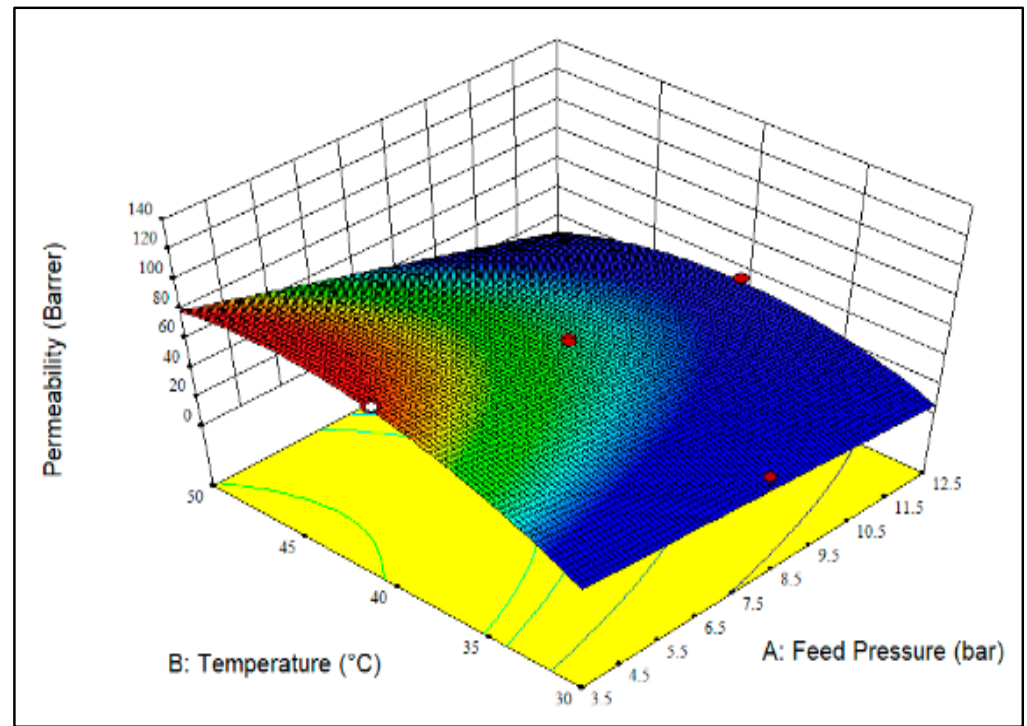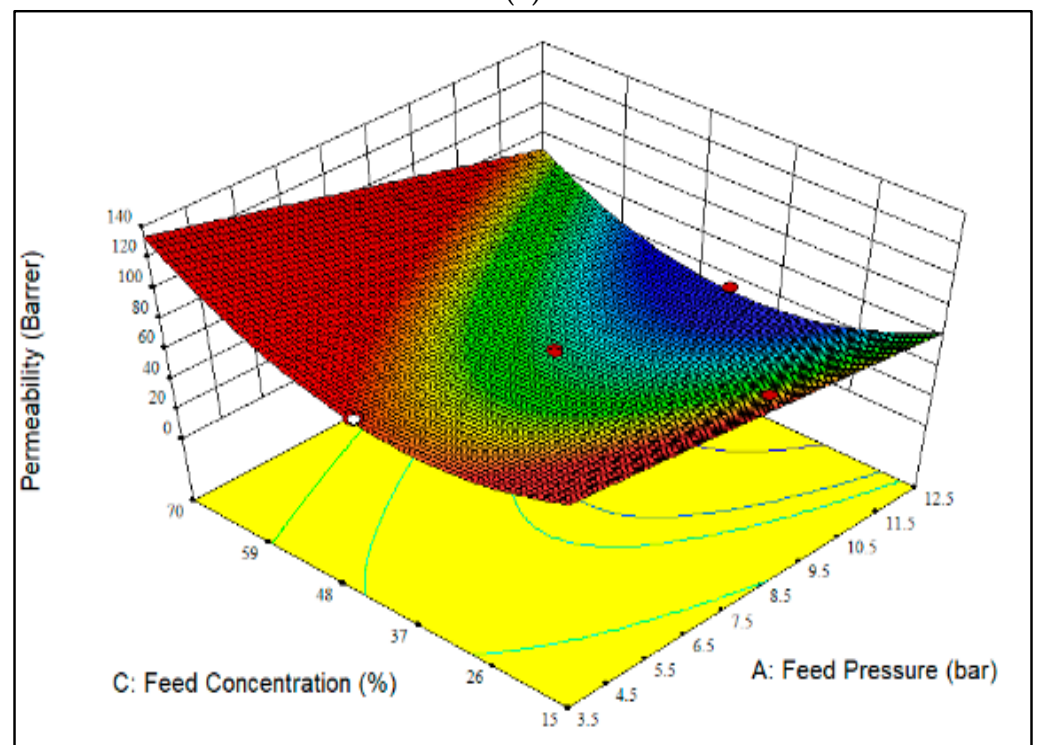
**Figure 2.** $CH_4$ permeability as a function of feed pressure, $CO_2$ feed concentration and temperature at (**a**) $CO_2$ feed concentration of 42.5 mol%, (**b**) temperature of 40 °C and (**c**) feed pressure of 8 bar. (The darker color (red) represents higher membrane performance whereas the lighter color (blue) indicated lower membrane performance.)

*3.5. $CO_2/CH_4$ Separation Factor*

The quadratic polynomial model for $CO_2/CH_4$ separation factor is defined in Equation (7) in the form of coded values.

$$Separation\ Factor_{coded} = 9.93 + 1.82A - 1.05B + 0.84C - 0.54AB + 0.46AC - 0.80BC + 0.30A^2 + 0.11B^2 - 2.70C^2 \tag{7}$$

where $A$, $B$ and $C$ denote the feed pressure (bar), temperature (°C) and $CO_2$ feed concentration (mol%), respectively.

The ANOVA analysis of the $CO_2/CH_4$ separation factor is presented in Table 5. It can be seen that model F and *p* values of 18.04 and <0.05 were achieved, respectively, indicating that the model terms are statistically significant, while *A*, *B*, *C*, *BC* and $C^2$ are statistically significant model terms. Furthermore, an $R^2$ value of 0.94 was achieved, showing the accuracy of the model for $CO_2/CH_4$ separation factor.

**Table 5.** Analysis of variance (ANOVA) for $CO_2/CH_4$ separation factor.

| Source | Sum of Squares | Degree of Freedom | Mean Square | F-Value | Prob > F |
|---|---|---|---|---|---|
| Model | 91.12 | 9 | 10.12 | 18.04 | <0.0001 [a] |
| A-Pressure | 33.27 | 1 | 33.27 | 59.29 | <0.0001 [a] |
| B-Temperature | 10.96 | 1 | 10.96 | 19.54 | 0.0013 [a] |
| C-Concentration | 7.12 | 1 | 7.12 | 12.69 | 0.0052 [a] |
| AB | 2.38 | 1 | 2.38 | 4.23 | 0.0666 [b] |
| AC | 1.71 | 1 | 1.71 | 3.05 | 0.1113 [b] |

**Table 5.** *Cont.*

| Source | Sum of Squares | Degree of Freedom | Mean Square | F-Value | Prob > F |
|--------|----------------|-------------------|-------------|---------|----------|
| BC | 5.18 | 1 | 5.18 | 9.24 | 0.0125 [a] |
| $A^2$ | 0.25 | 1 | 0.25 | 0.44 | 0.5229 [b] |
| $B^2$ | 0.036 | 1 | 0.036 | 0.064 | 0.8057 [b] |
| $C^2$ | 20.06 | 1 | 20.06 | 35.75 | 0.0001 [a] |
| Residual | 5.61 | 10 | 0.56 | | |
| Lack of Fit | 3.43 | 5 | 0.69 | 1.57 | 0.3168 [b] |
| $R^2$ | 0.94 | | | | |

[a] statistically significant, [b] statistically not significant.

Figure 3 displays 3D plots of the effect of feed pressure, temperature, and $CO_2$ feed concentration on the $CO_2/CH_4$ separation factor over the membrane. As shown, increasing the feed pressure resulted in a higher $CO_2/CH_4$ separation factor owing to the higher $CO_2$ adsorption capacity compared to $CH_4$, as well as the good compatibility of the polymer-filler, which was induced by the presence of $-NH_2$ groups in the membrane [27]. The enhanced $CO_2/CH_4$ separation factor was related to the improvement of $CO_2$ permeability and the reduction of $CH_4$ permeability observed in Figures 1a and 2a. In contrast, increasing the temperature revealed a negligible impact on $CO_2/CH_4$ separation factor, since the contribution of solubility and diffusivity is interchangeable. Additionally, as shown in Figure 3a, the highest $CO_2/CH_4$ separation factor, i.e., 13.0, was obtained at a temperature of 30 °C and a feed pressure of 12.5 bar. In comparison, the lowest $CO_2/CH_4$ separation factor, 7.3, was observed at a feed temperature of 50 °C and a feed pressure of 3.5 bar.

Figure 3b illustrates the effect of $CO_2$ feed concentration and feed pressure on the $CO_2/CH_4$ separation factor at a constant temperature of 40 °C. It can be observed that the $CO_2/CH_4$ separation factor increased with increasing feed pressure. This was mainly due to the higher sorption and permeation of $CO_2$ molecules over the membrane compared to $CH_4$ [33], which resulted in higher $CO_2$ permeability and lower $CH_4$ permeability, as observed in Figures 1b and 2b, respectively. The higher $CO_2$ permeability also contributed to the increase in $CO_2$ solubility and the reduction of $CH_4$ solubility, and thus, improved the $CO_2/CH_4$ solubility selectivity [36]. Furthermore, the $CO_2/CH_4$ separation factor displayed an increasing trend with increasing $CO_2$ feed concentration up to 42.5 mol%, and then decreased when the $CO_2$ feed concentration was increased further to 70 mol%. The increment of $CO_2$ feed concentration caused a reduction of $CH_4$ permeability and led to an increase in $CO_2/CH_4$ separation factor, owing to the smaller kinetic diameter of $CO_2$ compared to $CH_4$. Meanwhile, increasing the $CO_2$ feed concentration further from 42.5 mol% to 70 mol% caused an improvement of $CH_4$ permeability, but a reduction in the $CO_2/CH_4$ separation factor was observed due to the early stage of $CO_2$-induced plasticization behavior [33,37]. The highest separation factor, i.e., 13.0, was achieved at a feed pressure of 12.5 bar and $CO_2$ a feed concentration of 42.5 mol%. Meanwhile, the lowest $CO_2/CH_4$ separation factor, 6.0, was observed at a feed pressure of 3.5 bar and a $CO_2$ feed concentration of 15 mol%, mainly resulting from the presence of a larger amount of $CH_4$ gas (85 mol%) in the feed mixture.

Figure 3c shows the effect of $CO_2$ feed concentration and temperature on the $CO_2/CH_4$ separation factor at a pressure of 8 bar. From Figure 3c, increasing the temperature at a fixed feed pressure of 8 bar caused a slightly drop in the $CO_2/CH_4$ separation factor. This reduction was mainly due to the improvement of $CO_2$ and $CH_4$ permeability, as explained in Sections 3.3 and 3.4. Furthermore, at a fixed feed pressure of 8 bar, the increase of $CO_2$ feed concentration from 15 mol% to 42.5 mol% resulted in the enhancement of the $CO_2/CH_4$ separation factor, which was consistent with the increase of $CO_2$ permeability, as shown in Figure 1c. On the other hand, increasing the $CO_2$ feed concentration from 42.5 mol% to 70 mol% led to a slight drop in the $CO_2/CH_4$ separation factor due to the saturation of $CO_2$ gas molecules inside the polymer voids [11]. A parity plot for $CO_2/CH_4$

separation factor is shown in Figure S2c. Overall, the actual and predicted values of the responses were scattered near the 95% prediction limits. As shown in Figure S2c, very few data points fall outside the 95% prediction limits.
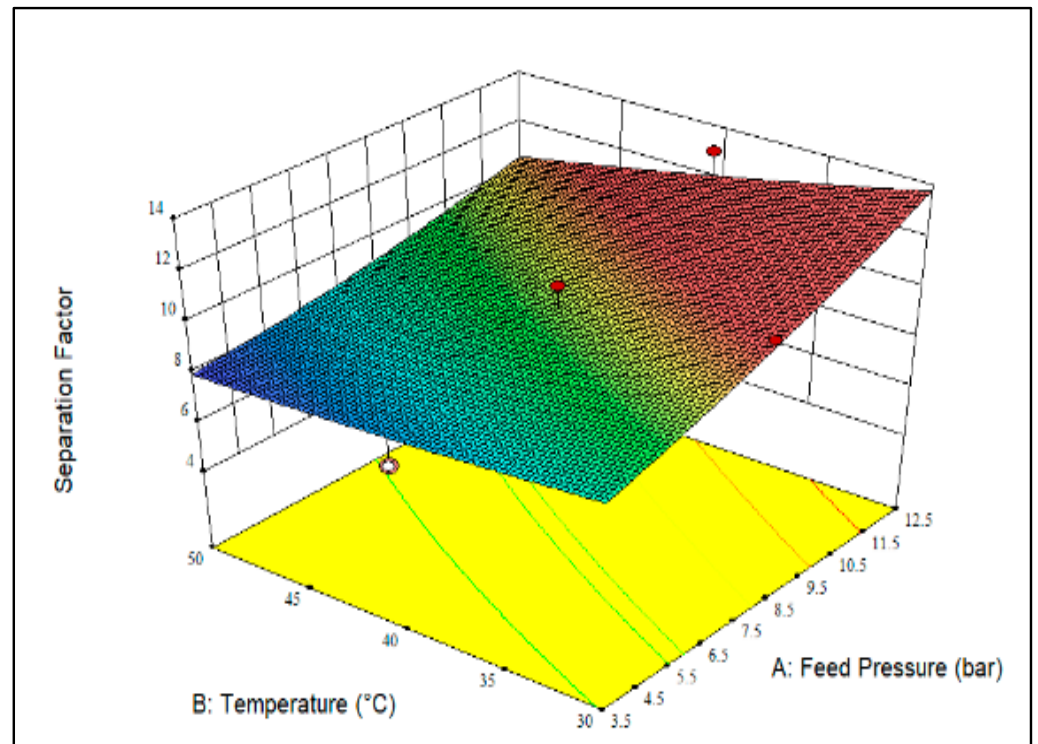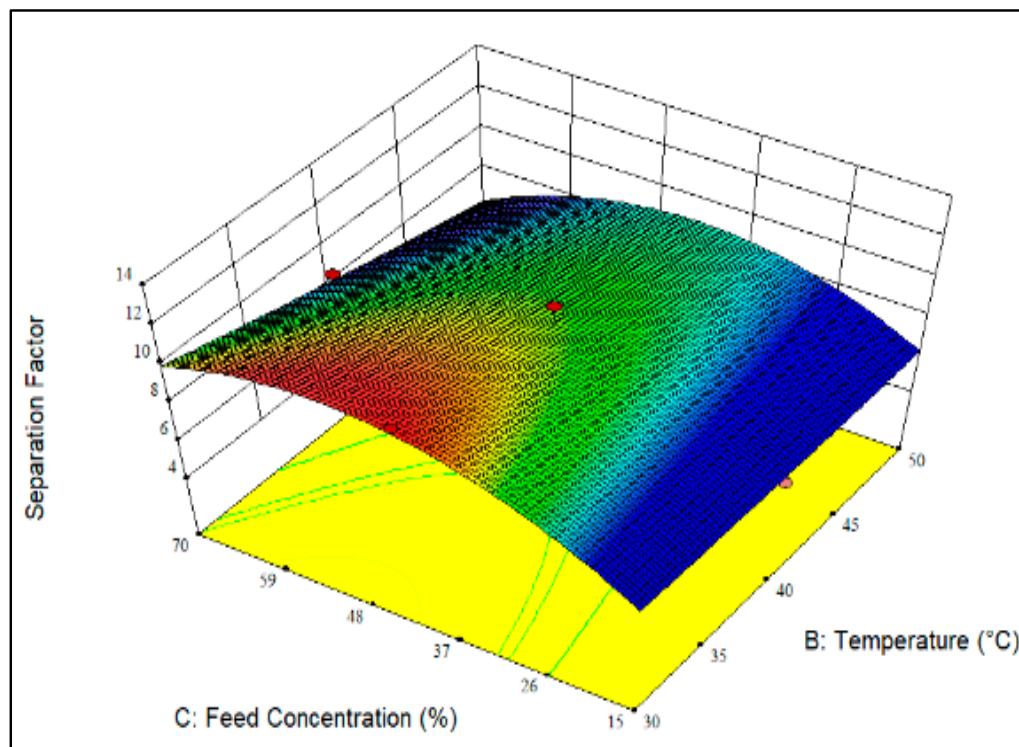


(**a**)
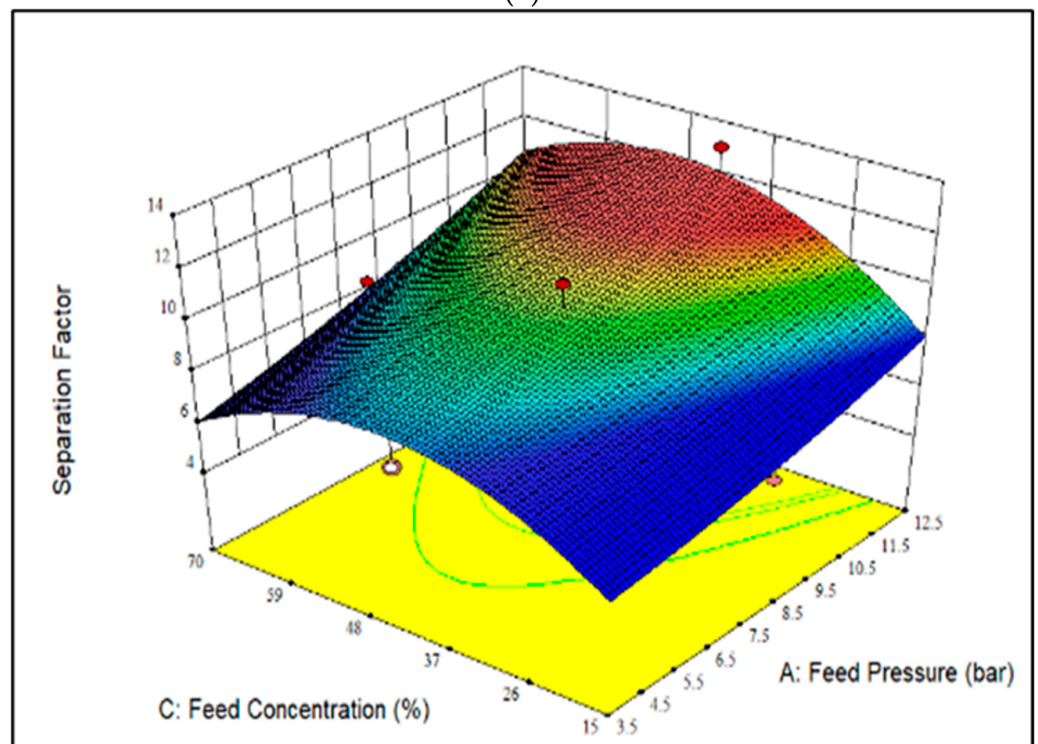


(**b**)

**Figure 3.** *Cont.*

**(c)**

**Figure 3.** 3D surface of the $CO_2/CH_4$ separation factor as a function of feed pressure, $CO_2$ feed concentration and temperature at (**a**) $CO_2$ feed concentration of 42.5 mol%, (**b**) temperature of 40 °C and (**c**) feed pressure of 8 bar. (The darker colour (red) represents higher membrane performance whereas the lighter color (blue) indicates lower membrane performance.).

*3.6. Optimization of $CO_2/CH_4$ Separation Performance*

The primary objective of this work is to identify the optimal operational conditions for membrane separation in terms of $CO_2$ permeability and $CO_2/CH_4$ separation factor. Therefore, the optimization conditions included maximizing the $CO_2$ feed concentration as an operational parameter, as well as $CO_2$ permeability and $CO_2/CH_4$ separation factor. Additionally, the desirability function (DF) was used in RSM to optimize a sequence of quadratic models. The geometric mean of individual desirability (d) was used to calculate the total desirability (D), as expressed in Equation (8) [38]:

$$D_d = (d_1 \times d_2 \times \ldots d_n)^{\frac{1}{n}} \tag{8}$$

where $D_d$ is the total desirability and $d_n$ is the nth desirability, $n = 1, 2, \ldots,$ n. The total desirability was measured from 0 to 1, where 0 represents the most undesirable response and 1 the most desirable.

The optimum solution and its desirability generated by the DOE software is listed in Table 6 in term of actual values. The optimum operational parameters suggested for $CO_2$ feed concentration, feed pressure, and temperature were 70 mol%, 12.5 bar and 34.7 °C, respectively, which yielded optimal $CO_2$ permeability and separation factor values, i.e., 571.9 Barrer and 11.9, respectively.

**Table 6.** Experimental conditions generated by the DOE software and responses.

| Pressure (bar) | Temperature (°C) | Concentration (mol%) | $CO_2$ Permeability (Barrer) | $CH_4$ Permeability (Barrer) | $CO_2/CH_4$ Separation Factor | Desirability |
|---|---|---|---|---|---|---|
| 12.5 | 34.7 | 70.0 | 571.9 | 60.4 | 11.9 | 0.8 |

*3.7. Validation of the Optimum Condition*

In order to validate the optimum conditions and predicted responses shown in Table 6, three repeated experiments were conducted based on the suggested conditions; the results are presented in Table 7. The percentage (%) error for $CO_2$ permeability ranged from 3.6% to 6.5% relative to the standard deviation of 1.5%. On the other hand, the percentage (%) error for $CO_2/CH_4$ separation factor ranged from 0.8% to 5.0% with a standard deviation of 2.1%. Meanwhile, the average errors obtained for $CO_2$ permeability and $CO_2/CH_4$ separation factor were 5.3% and 2.8%, respectively. Overall, the average error for the experimental and predicted values were within 5%, indicating that the model validity reached 95% of the prediction interval. Consequently, the model was successfully validated, and as such, the optimization of operational parameters was achieved utilizing the RSM approach.

**Table 7.** Validation of optimal condition for membrane separation.

| Run | CO$_2$ Permeability | | | Separation Factor | | |
|---|---|---|---|---|---|---|
| | Actual (Barrer) | Predicted (Barrer) | Error (%) | Actual | Predicted | Error (%) |
| 1 | 609.3 | 571.9 | 6.5 | 11.6 | 11.9 | 2.5 |
| 2 | 592.7 | 571.9 | 3.6 | 11.8 | 11.9 | 0.8 |
| 3 | 605.3 | 571.9 | 5.8 | 11.3 | 11.9 | 5.0 |
| Average (%) | | | 5.3 | Average (%) | | 2.8 |
| Standard deviation | | | 1.5 | Standard deviation | | 2.1 |

## 4. Conclusions

In conclusion, the effects of operational parameters, i.e., feed pressure, temperature and $CO_2$ feed concentration, were identified as dominant factors influencing the separation performance of a NH$_2$-MIL-125 (Ti)-6FDA/durene membrane. $CO_2$ feed concentration demonstrated a significant effect on $CO_2$ permeability, whereas feed pressure was the primary parameter influencing $CH_4$ permeability and $CO_2/CH_4$ separation factor, with F-values of 102.5 and 59.3, respectively. The $R^2$ values obtained ranged from 0.94 to 0.96, indicating that the regression models were statistically significant. The optimum operational parameters, i.e., a feed pressure of 12.5 bar, a temperature of 34.7 °C and a $CO_2$ feed concentration of 70 mol%, yielded the maximum $CO_2$ permeability, i.e., 609.3 Barrer, and a $CO_2/CH_4$ separation factor of 11.6. The average errors for $CO_2$ permeability and $CO_2/CH_4$ separation factor were 5.3% and 2.8%, respectively, suggesting that the model was 95% reliable. Overall, the experimental findings show that the RSM paired with the CCD method is a better strategy to obtain optimal $CO_2/CH_4$ separation performance with a NH$_2$-MIL-125 (Ti)/6FDA-based mixed matrix membrane. The present research provides an experimental reference for further improvements and scale-ups of membranes in $CO_2/CH_4$ separation with high $CO_2$ feed concentrations.

## References

1.  Sukor, N.R.; Shamsuddin, A.H.; Mahlia, T.M.I.; Mat Isa, M.F. Techno-Economic Analysis of $CO_2$ Capture Technologies in Offshore Natural Gas Field: Implications to Carbon Capture and Storage in Malaysia. *Processes* **2020**, *8*, 350. [CrossRef]
2.  Wang, Z.; Yuan, J.; Li, R.; Zhu, H.; Duan, J.; Guo, Y.; Liu, G.; Jin, W. ZIF-301 MOF/6FDA-DAM polyimide mixed-matrix membranes for $CO_2$/$CH_4$ separation. *Sep. Purif. Technol.* **2021**, *264*, 118431. [CrossRef]
3.  Suhaimi, N.H.; Yeong, Y.F.; Jusoh, N.; Chew, T.L.; Bustam, M.A.; Suleman, S. Separation of $CO_2$ from $CH_4$ using mixed matrix membranes incorporated with amine functionalized MIL-125 (Ti) nanofiller. *Chem. Eng. Res. Des.* **2020**, *159*, 236–247. [CrossRef]
4.  Peters, L.; Hussain, A.; Follmann, M.; Melin, T.; Hägg, M.B. $CO_2$ removal from natural gas by employing amine absorption and membrane technology—A technical and economical analysis. *Chem. Eng. J.* **2011**, *172*, 952–960. [CrossRef]
5.  Alonso, A.; Moral-Vico, J.; Abo Markeb, A.; Busquets-Fite, M.; Komilis, D.; Puntes, V.; Sanchez, A.; Font, X. Critical review of existing nanomaterial adsorbents to capture carbon dioxide and methane. *Sci. Total Environ.* **2017**, *595*, 51–62. [CrossRef] [PubMed]
6.  Mubashir, M.; Dumee, L.F.; Fong, Y.Y.; Jusoh, N.; Lukose, J.; Chai, W.S.; Show, P.L. Cellulose acetate-based membranes by interfacial engineering and integration of ZIF-62 glass nanoparticles for $CO_2$ separation. *J. Hazard. Mater.* **2021**, *415*, 125639. [CrossRef] [PubMed]
7.  Yu, L.; Kanezashi, M.; Nagasawa, H.; Tsuru, T. Role of Amine Type in $CO_2$ Separation Performance within Amine Functionalized Silica/Organosilica Membranes: A Review. *Appl. Sci.* **2018**, *8*, 1032. [CrossRef]
8.  Liu, N.; Cheng, J.; Hou, W.; Yang, X.; Luo, M.; Zhang, H.; Ye, B.; Zhou, J. Mg2(dobdc) crystals adhere to Matrimid matrix membranes bridged by diethylenetriamine (DETA) as an adhesion agent for efficient $CO_2$ separation. *Sep. Purif. Technol.* **2022**, *278*, 119635. [CrossRef]
9.  Zagho, M.M.; Hassan, M.K.; Khraisheh, M.; Al-Maadeed, M.A.A.; Nazarenko, S. A review on recent advances in $CO_2$ separation using zeolite and zeolite-like materials as adsorbents and fillers in mixed matrix membranes (MMMs). *Chem. Eng. J. Adv.* **2021**, *6*, 100091. [CrossRef]
10. Baneshi, M.M.; Ghaedi, A.M.; Vafaei, A.; Emadzadeh, D.; Lau, W.J.; Marioryad, H.; Jamshidi, A. A high-flux P84 polyimide mixed matrix membranes incorporated with cadmium-based metal organic frameworks for enhanced simultaneous dyes removal: Response surface methodology. *Environ. Res.* **2020**, *183*, 109278. [CrossRef]
11. Mashhadikhan, S.; Ebadi Amooghin, A.; Moghadassi, A.; Sanaeepur, H. Functionalized filler/synthesized 6FDA-Durene high performance mixed matrix membrane for $CO_2$ separation. *J. Ind. Eng. Chem.* **2021**, *93*, 482–494. [CrossRef]
12. Ahmadipouya, S.; Ahmadijokani, F.; Molavi, H.; Rezakazemi, M.; Arjmand, M. $CO_2$/$CH_4$ Separation by Mixed-Matrix Membranes holding Functionalized $NH_2$-MIL-101(Al) Nanoparticles: Effect of Amino-Silane Functionalization. *Chem. Eng. Res. Des.* **2021**, *176*, 49–59. [CrossRef]
13. Suhaimi, N.H.; Yeong, Y.F.; Ch'ng, C.W.M.; Jusoh, N. Tailoring $CO_2$/$CH_4$ Separation Performance of Mixed Matrix Membranes by Using ZIF-8 Particles Functionalized with Different Amine Groups. *Polymer* **2019**, *11*, 2042. [CrossRef] [PubMed]
14. Chuah, C.Y.; Li, W.; Samarasinghe, S.A.S.C.; Sethunga, G.S.M.D.P.; Bae, T.-H. Enhancing the $CO_2$ separation performance of polymer membranes via the incorporation of amine-functionalized HKUST-1 nanocrystals. *Microporous Mesoporous Mater.* **2019**, *290*, 109680. [CrossRef]
15. Meshkat, S.; Kaliaguine, S.; Rodrigue, D. Mixed matrix membranes based on amine and non-amine MIL-53(Al) in Pebax®MH-1657 for $CO_2$ separation. *Sep. Purif. Technol.* **2018**, *200*, 177–190. [CrossRef]
16. Waqas Anjum, M.; Bueken, B.; De Vos, D.; Vankelecom, I.F.J. MIL-125(Ti) based mixed matrix membranes for $CO_2$ separation from $CH_4$ and $N_2$. *J. Membr. Sci.* **2016**, *502*, 21–28. [CrossRef]
17. Guo, X.; Huang, H.; Ban, Y.; Yang, Q.; Xiao, Y.; Li, Y.; Yang, W.; Zhong, C. Mixed matrix membranes incorporated with amine-functionalized titanium-based metal-organic framework for $CO_2$/$CH_4$ separation. *J. Membr. Sci.* **2015**, *478*, 130–139. [CrossRef]
18. Taheri Afarani, H.; Sadeghi, M.; Moheb, A.; Esfahani, E.N. Optimization of the gas separation performance of polyurethane–zeolite 3A and ZSM-5 mixed matrix membranes using response surface methodology. *Chin. J. Chem. Eng.* **2019**, *27*, 110–129. [CrossRef]

19. Mubashir, M.; Yeong, Y.F.; Leng, C.T.; Keong, L.K.; Jusoh, N. Study on the effect of process parameters on $CO_2/CH_4$ binary gas separation performance over $NH_2$-MIL-53(Al)/cellulose acetate hollow fiber mixed matrix membrane. *Polym. Test.* **2020**, *81*, 106223. [CrossRef]

20. Jusoh, N.; Yeong, Y.F.; Lau, K.K.; Shariff, A. Transport properties of mixed matrix membranes encompassing zeolitic imidazolate framework 8 (ZIF-8) nanofiller and 6FDA-durene polymer: Optimization of process variables for the separation of $CO_2$ from $CH_4$. *J. Clean. Prod.* **2017**, *149*, 80–95. [CrossRef]

21. Jusoh, N.; Yeong, Y.F.; Cheong, W.L.; Lau, K.K.; Shariff, A. Facile fabrication of mixed matrix membranes containing 6FDA-durene polyimide and ZIF-8 nanofillers for $CO_2$ capture. *J. Ind. Eng. Chem.* **2016**, *44*, 164–173. [CrossRef]

22. Zamidi Ahmad, M.; Navarro, M.; Lhotka, M.; Zornoza, B.; Téllez, C.; Fila, V.; Coronas, J. Enhancement of $CO_2/CH_4$ separation performances of 6FDA-based co-polyimides mixed matrix membranes embedded with UiO-66 nanoparticles. *Sep. Purif. Technol.* **2018**, *192*, 465–474. [CrossRef]

23. Sainath, K.; Modi, A.; Bellare, J. $CO_2/CH_4$ mixed gas separation using graphene oxide nanosheets embedded hollow fiber membranes: Evaluating effect of filler concentration on performance. *Chem. Eng. J. Adv.* **2021**, *5*, 100074. [CrossRef]

24. Jiang, Y.; Liu, C.; Caro, J.; Huang, A. A new UiO-66-$NH_2$ based mixed-matrix membranes with high $CO_2/CH_4$ separation performance. *Microporous Mesoporous Mater.* **2019**, *274*, 203–211. [CrossRef]

25. Maghami, S.; Mehrabani-Zeinabad, A.; Sadeghi, M.; Sánchez-Laínez, J.; Zornoza, B.; Téllez, C.; Coronas, J. Mathematical modeling of temperature and pressure effects on permeability, diffusivity and solubility in polymeric and mixed matrix membranes. *Chem. Eng. Sci.* **2019**, *205*, 58–73. [CrossRef]

26. Shahid, S.; Baron, G.V.; Denayer, J.F.M.; Martens, J.A.; Wee, L.H.; Vankelecom, I.F.J. Hierarchical ZIF-8 composite membranes: Enhancing gas separation performance by exploiting molecular dynamics in hierarchical hybrid materials. *J. Membr. Sci.* **2021**, *620*, 118943. [CrossRef]

27. Mozafari, M.; Rahimpour, A.; Abedini, R. Exploiting the effects of zirconium-based metal organic framework decorated carbon nanofibers to improve $CO_2/CH_4$ separation performance of thin film nanocomposite membranes. *J. Ind. Eng. Chem.* **2020**, *85*, 102–110. [CrossRef]

28. Li, P.; Chung, T.S.; Paul, D.R. Gas sorption and permeation in PIM-1. *J. Membr. Sci.* **2013**, *432*, 50–57. [CrossRef]

29. Salahshoori, I.; Seyfaee, A.; Babapoor, A.; Neville, F.; Moreno-Atanasio, R. Evaluation of the effect of silica nanoparticles, temperature and pressure on the performance of $PSF/PEG/SiO_2$ mixed matrix membranes: A molecular dynamics simulation (MD) and design of experiments (DOE) study. *J. Mol. Liq.* **2021**, *333*, 115957. [CrossRef]

30. Molki, B.; Aframehr, W.M.; Bagheri, R.; Salimi, J. Mixed matrix membranes of polyurethane with nickel oxide nanoparticles for $CO_2$ gas separation. *J. Membr. Sci.* **2018**, *549*, 588–601. [CrossRef]

31. Cheng, Y.; Ying, Y.; Zhai, L.; Liu, G.; Dong, J.; Wang, Y.; Christopher, M.P.; Long, S.; Wang, Y.; Zhao, D. Mixed matrix membranes containing MOF@COF hybrid fillers for efficient $CO_2/CH_4$ separation. *J. Membr. Sci.* **2019**, *573*, 97–106. [CrossRef]

32. Soltani, B.; Asghari, M. Effects of ZnO Nanoparticle on the Gas Separation Performance of Polyurethane Mixed Matrix Membrane. *Membrane* **2017**, *7*, 43. [CrossRef] [PubMed]

33. Ahmad, M.Z.; Peters, T.A.; Konnertz, N.M.; Visser, T.; Téllez, C.; Coronas, J.; Fila, V.; de Vos, W.M.; Benes, N.E. High-pressure $CO_2/CH_4$ separation of Zr-MOFs based mixed matrix membranes. *Sep. Purif. Technol.* **2020**, *230*, 115858. [CrossRef]

34. Kida, K.; Maeta, Y.; Yogo, K. Pure silica CHA-type zeolite membranes for dry and humidified $CO_2/CH_4$ mixtures separation. *Sep. Purif. Technol.* **2018**, *197*, 116–121. [CrossRef]

35. Ricci, E.; Gemeda, A.E.; Du, N.; Li, N.; De Angelis, M.G.; Guiver, M.D.; Sarti, G.C. Sorption of $CO_2/CH_4$ mixtures in TZ-PIM, PIM-1 and PTMSP: Experimental data and NELF-model analysis of competitive sorption and selectivity in mixed gases. *J. Membr. Sci.* **2019**, *585*, 136–149. [CrossRef]

36. Genduso, G.; Wang, Y.; Ghanem, B.S.; Pinnau, I. Permeation, sorption, and diffusion of $CO_2$-$CH_4$ mixtures in polymers of intrinsic microporosity: The effect of intrachain rigidity on plasticization resistance. *J. Membr. Sci.* **2019**, *584*, 100–109. [CrossRef]

37. Zhang, M.; Deng, L.; Xiang, D.; Cao, B.; Hosseini, S.; Li, P. Approaches to Suppress $CO_2$-Induced Plasticization of Polyimide Membranes in Gas Separation Applications. *Processes* **2019**, *7*, 51. [CrossRef]

38. Karimnezhad, H.; Navarchian, A.H.; Tavakoli Gheinani, T.; Zinadini, S. Amoxicillin removal by Fe-based nanoparticles immobilized on polyacrylonitrile membrane: Effects of input parameters and optimization by response surface methodology. *Chem. Eng. Processing Process Intensif.* **2020**, *147*, 107785. [CrossRef]